OPEN ACCESS
Freely Available Online

JOURNAL OF NEW DEVELOPMENTS IN CHEMISTRY
ISSN NO: 2377-2549

Research Article

DOI: 10.14302/issn.2377-2549.jndc-21-3722

# Evaluation of Physicochemical, Spectral and Thermal Properties of Energy of Consciousness Healing Treated Iron Sulphate

Mahendra Kumar Trivedi[1], Snehasis Jana[2, *]

[1]Trivedi Global, Inc., Henderson, Nevada, USA

[2]Trivedi Science Research Laboratory Pvt. Ltd., Thane (W), India

**Abstract**

Iron sulphate is used in the treatment of iron deficiency anaemia and other chronic disorders such as heart and kidney diseases. This study has the objective to analyze the impact of The Trivedi Effect®-Energy of Consciousness Healing Treatment on the physicochemical, spectroscopic and thermal properties of iron sulphate using various analytical techniques. In this, the test compound, *i.e.,* iron sulphate was divided into two parts; one as control (without Biofield Energy Treatment), and the other as Biofield Energy Treated, which received the Biofield Energy Treatment remotely by the renowned Healer, Mr. Mahendra Kumar Trivedi. The PXRD analysis of the Biofield Energy Treated sample showed significant alterations in the range of -39.49 to 301.40% in the relative intensities, and from -15.40 to 33.36% in the crystallite sizes, compared with the control sample. The average crystallite size of the treated sample was also increased by 4.98% as compared to the control sample. The particle sizes in the treated sample at $d_{10}$, $d_{50}$, $d_{90}$ and D(4,3) values were significantly increased by 67.12%, 47.72%, 33.18% and 42.01%, respectively; whereas, the specific surface area was significantly reduced by 38.39%, compared with the control sample. The TGA thermograms showed three steps of thermal degradation in which, the weight loss of Biofield Energy Treated sample in the first and second step was reduced by 5.82% and 16.09%, respectively, while, it was increased by 6.78% in the third step, compared to the control sample. The total weight loss in the treated sample was also reduced by 2.76%, along with slight alteration in the maximum thermal decomposition temperature, compared with the control sample. The DSC analysis showed the decrease in the melting temperatures of the 1$^{st}$, 2$^{nd}$ and 4$^{th}$ peaks by 8.24%, 19.29%, and 0.61%, respectively, while 4.57% increase in the 3$^{rd}$ peak of the treated sample, compared with the control sample. The latent heat of fusion (ΔH) corresponding to the 1$^{st}$, 2$^{nd}$, 3$^{rd}$ and 4$^{th}$ peaks of the treated sample also showed alterations by -92.29, -86.29, 60.92, and 6.37%, respectively, compared with the control sample. The Trivedi Effect®-Consciousness Energy Healing Treatment might produce a novel polymorphic form of iron sulphate having increased crystallite and particle size along with enhanced thermal stability. It may help in improving the quality, safety and stability during the process of handling, storage, and shipment of the iron sulphate with better therapeutic response against iron deficiency anaemia.

OPEN ACCESS
Freely Available Online

OpenAccessPub

**Corresponding author:** Snehasis Jana, Trivedi Science Research Laboratory Pvt. Ltd., Thane (W), India.
Tel: +91- 022-25811234

**Citation:** Mahendra Kumar Trivedi, Snehasis Jana (2021) Evaluation of Physicochemical, Spectral and Thermal Properties of Energy of Consciousness Healing Treated Iron Sulphate. Journal of New Developments in Chemistry - 3(2):50-68. https://doi.org/10.14302/issn.2377-2549.jndc-21-3722

**Keywords:** Iron sulphate, Energy of Consciousness Healing Treatment, The Trivedi Effect®, PXRD, PSA, TGA/DTG, DSC

**Received:** Jan 22, 2021 **Accepted:** Feb 08, 2021 **Published:** Feb 09, 2021

**Editor:** Zhe-Sheng Chenz, Department of Pharmaceutical Sciences, College of Pharmacy and Allied Health Professions, St. John's University , United States.

## Introduction

Iron is an essential component of human body due to its important role in the transport as well as the storage of oxygen. It is necessary for cellular growth and proliferation and also acts as the electron carrier for various enzymes and catalyst regarding the process of oxygenation and hydroxylation [1]. However, the iron deficiency and iron deficiency anaemia (IDA) are the most frequent global nutritional disorders [2]. IDA may create severe problems during pregnancy that include the preterm delivery, maternal postpartum depression, perinatal mortality, and impeded cognitive ability and mental development of the child [3]. Thus, it is treated by using solid or liquid iron supplements, usually in the form of ferrous salt such as ferrous sulphate, ferrous gluconate, or ferrous fumarate [4]. Apart from that, the iron supplements are also used during the treatment of some chronic diseases such as heart failure, kidney disease, or inflammatory bowel disease [5-7].

Besides, sulphate is another important nutrient that is required for the growth and development of fetus. Various researches established the importance of sulphate in the process of fertilization and pregnancy. It contributes in the maturation of oocyte through which the zona pellucida becomes able to accept sperm [8, 9]. Although, nearly one third of required sulphate is obtained through food [10], however, its intake in the adults and children may vary depending on the types of consumed food and the drinking water source [11, 12]. Thus, it also requires the supplements to fulfill the needs. Several studies have been done on the various iron preparations such as, conventional, modified-release, and fast-release iron sulphate tablets; among which modified-release or other formulations showed poor bioavailability [13-15]. In this regard, the Biofield Energy Treatment is considered as the consequential approach for its impact on the bioavailability profile of drugs.

Biofield Energy is a cumulative form of electromagnetic field, exerted by the human body [16] *via* various internal processes such as blood flow, lymph flow, brain functions, and heart function. However, various hypothetical vital forces such as prana by the Hindus, *qi* or *chi* by the Chinese, and *ki* by the Japanese has been scientifically evaluated and is now considered the Bioenergetics Field [17]. Biofield Energy can be transmitted into any living organism(s) or nonliving object(s) around the globe [18]. The object or recipient always receives the energy and responds in a useful way. This process is known as The Trivedi Effect®- Biofield Energy Healing Treatment [19]. Various scientific studies reported that Biofield Energy Healing have significant outcomes which showed more effective alternative, respective to other approaches [20].

Complementary and Alternative Medicine (CAM) therapies have been increasing day-by-day worldwide among which Biofield Therapy (or Healing Modalities) have been reported to have several benefits to enhance physical, mental, and emotional human wellness. Biofield (Putative Energy Field) based Energy Therapies have been emerging worldwide to promote health and healing. The National Center of Complementary and Integrative Health (NCCIH) has recognized and accepted Biofield Energy Healing as CAM approach in addition to other therapies, medicines and practices such as natural products, deep breathing, yoga, Tai Chi, Qi Gong, chiropractic/osteopathic manipulation, meditation, massage, special diets, homeopathy, progressive relaxation, guided imagery, acupressure, acupuncture, relaxation techniques, hypnotherapy,

healing touch, movement therapy, pilates, rolfing structural integration, mindfulness, ayurvedic medicine, traditional Chinese herbs and medicines, naturopathy, essential oils, aromatherapy, Reiki, cranial sacral therapy and applied prayer in various religions [21]. The Trivedi Effect®-Biofield Energy Consciousness Healing Treatment have been reported scientifically to transform the characteristic properties of living organism and non-living substances in the field of microbiology [22-24], cancer cells [25], agricultural crops [26-28], pharmaceutical medium [29, 30], material science [31, 32], pharmaceutical compounds [33, 34], nutraceutical [35-37], and organic compounds [38-40]. Hence, the current study was aimed to determine the impact of Biofield Energy Treatment on the physicochemical, spectral, and thermal properties of iron sulphate.

## Materials and Methods

### *Chemicals and Reagents*

Ferrous sulphate heptahydrate or iron (II) sulphate heptahydrate (>99%) was purchased from Sigma-Aldrich, India. All other chemicals used during the experiments were of analytical grade available in India.

### *Consciousness Energy Healing Treatment Strategies*

The test compound *i.e.,* iron sulphate was taken and separated into two different parts. In one part, no treatment was given and the sample was considered as control iron sulphate. Besides, in the other part, the Energy of Consciousness Healing Treatment was provided by the renowned Biofield Energy Healer, Mr. Mahendra Kumar Trivedi (USA), and the sample was named as the Biofield Energy Treated iron sulphate. In the process of Biofield Energy Treatment, the sample was placed under the standard laboratory conditions and the Healer remotely provided the Trivedi Effect® - Energy of Consciousness Healing Treatment to the sample for 3 minutes through the Unique Energy Transmission process. Consequently, the control sample was subjected under the similar laboratory conditions to "sham" healer, who did not have any knowledge about the Biofield Energy Treatment. Later on, both the control and Biofield Energy Treated samples were kept in similar sealed conditions and characterized by using various analytical techniques such as PXRD, PSA, UV-Vis, FT-IR, TGA/DTG, and DSC techniques for analyzing the impact of Biofield Energy Treatment on the iron sulphate sample.

### *Characterization*

#### *Powder X-ray Diffraction (PXRD) Analysis*

The PXRD analysis of the control and Biofield Energy Treated samples of iron sulphate was done using PANalytical X'Pert3 powder X-ray diffractometer, UK. The copper line was used as the source of radiation for diffraction of the analyte at 0.154 nm X-ray wavelength that is running at 40 mA current and 45 kV voltage. The instrument uses a scanning rate of 18.87°/second over a 2q range of 3-90° and the ratio of Kα-2 and Kα-1 was 0.5 (k, equipment constant). The data was collected using X'Pert data collector and X'Pert high score plus processing software in the form of a chart of the Bragg angle (2θ) *vs.* intensity (counts per second), and a detailed table containing information on peak intensity counts, d value (Å), full width half maximum (FWHM) (° 2θ), relative intensity (%), and area (cts*°2θ). The crystallite size (G) was calculated by using the Scherrer equation (1) as follows:

$$G = k\lambda/(b\cos\theta) \quad (1)$$

Where, k is the equipment constant (0.5), λ is the X-ray wavelength (0.154 nm); b in radians is the full -width at half of the peaks and θ is the corresponding Bragg angle.

Percent change in crystallite size (G) of iron sulphate was calculated using following equation 2:

$$\%\ \text{change in crystallite size} = \frac{[G_{\text{Treated}} - G_{\text{Control}}]}{G_{\text{Control}}} \times 100 \quad ...(2)$$

Where, $G_{Control}$ and $G_{Treated}$ are the crystallite size of the control and Biofield Energy Treated iron sulphate samples, respectively.

### *Particle Size Analysis (PSA)*

The particle size analysis involves wet method, which is done using Malvern Mastersizer 3000, UK. The instrument has a detection range between 0.01 µm to 3000 µm [41], and the method involves the filling of sample unit (Hydro MV) with light liquid paraffin oil, which acts as dispersant medium. Further, it was stirred at 2500 rpm. The refractive index values for dispersant

medium and samples were 0.0 and 1.47, respectively. The measurement was taken twice after reaching obscuration in between 10% and 20%, and the average of both the measurements were done consequently. The PS analysis provides data in the form of $d_{10}$ µm, $d_{50}$ µm, and $d_{90}$ µm, representing the particle diameter corresponding to 10%, 50%, and 90% of the cumulative distribution. D(4, 3) µm represents the average mass-volume diameter and SSA is the specific surface area ($m^2$/Kg). The calculations were done by using software Mastersizer V3.50.

The percent change in particle size (d) for $d_{10}$, $d_{50}$, $d_{90}$ and D(4,3) was calculated using following equation 3:

$$\% \text{ change in particle size} = \frac{[d_{Treated} - d_{Control}]}{d_{Control}} \times 100 \quad ...(3)$$

Where, $d_{Control}$ and $d_{Treated}$ are the particle size (µm) for at below 10% level ($d_{10}$), 50% level ($d_{50}$), and 90% level ($d_{90}$) of the control and Biofield Energy Treated samples, respectively.

Percent change in surface area (S) was calculated using following equation 4:

$$\% \text{ change in surface area} = \frac{[S_{Treated} - S_{Control}]}{S_{Control}} \times 100 \quad ...(4)$$

Where, $S_{Control}$ and $S_{Treated}$ are the surface area of the control and Biofield Energy treated iron (II)sulphate, respectively.

*Ultraviolet-visible Spectroscopy (UV-Vis) Analysis*

The UV-Vis spectral analysis of the control and Biofield Energy Treated iron sulphate samples was carried out using Shimadzu UV-2400PC SERIES with UV Probe (Shimadzu, JAPAN). The spectrum was recorded in the wavelength range of 190-800 nm using 1 cm quartz cell having a slit width of 0.5 nm. The absorbance spectra (in the range of 0.2 to 0.9) and wavelength of maximum absorbance ($\lambda_{max}$) were recorded.

*Fourier Transform Infrared (FT-IR) Spectroscopy*

FT-IR spectroscopy of iron (II) sulphate was performed on Spectrum ES Fourier transform infrared spectrometer (Perkin Elmer, USA) by using pressed KBr disk technique with the frequency array of 400-4000 $cm^{-1}$. The technique uses ~2 mg of the control sample and about 300 mg of KBr as the diluent to form the pressed disk followed by running the sample in the spectrometer. The same procedure was used for the Biofield Energy Treated sample.

*Thermal Gravimetric Analysis (TGA) / Differential Thermogravimetric Analysis (DTG)*

TGA/DTG thermograms of control and Biofield Energy Treated iron sulphate samples were obtained using TGA Q500 themoanalyzer apparatus, USA under dynamic nitrogen atmosphere (50 mL/min). It involves the heating rate of 10 ºC/min from 25 °C to 800 °C and uses platinum crucible [42]. In TGA analysis, the weight loss in gram as well as percent loss for each step was recorded with respect to the initial weight of the sample. Later on, in DTG analysis, the onset, endset, peak temperature and integral area for each peak was recorded. The percent change in weight loss (W) was calculated using following equation 5:

$$\% \text{ change in weight loss} = \frac{[W_{Treated} - W_{Control}]}{W_{Control}} \times 100 \quad ...(5)$$

Where, $W_{Control}$ and $W_{Treated}$ are the weight loss of the control and Biofield Energy Treated samples, respectively.

Also, the percent change in maximum thermal degradation temperature ($T_{max}$) (M) was calculated using following equation 6:

$$\% \text{ change in } T_{max} \text{ (M)} = \frac{[M_{Treated} - M_{Control}]}{M_{Control}} \times 100 \quad ...(6)$$

Where, $M_{Control}$ and $M_{Treated}$ are the $T_{max}$ values of the control and Biofield Energy Treated samples, respectively.

*Differential Scanning Calorimetry (DSC)*

The DSC analysis of the samples was performed using DSC Q2000 differential scanning calorimeter, USA under the dynamic nitrogen atmosphere with flow rate of 50 mL/min. For analysis, 2-4 mg sample was weighed and sealed in aluminium pans. Further, it was equilibrated at 30°C and heated up to 450ºC at the heating rate of 10º C/min under Nitrogen gas as purge atmosphere [42]. The value for onset, end set, peak temperature, peak height (mJ or mW), peak area, and change in heat (J/g) for each peak was recorded. Later on, the percent change in melting temperature (T) of the control and Biofield Energy Treated samples was

calculated using following equation 7:

$$\% \text{ change in melting temperature} = \frac{[T_{Treated} - T_{Control}]}{T_{Control}} \times 100 \quad (7)$$

Where, $T_{Control}$ and $T_{Treated}$ are the melting temperature of the control and Biofield Energy Treated iron sulphate samples, respectively.

Also, the percent change in the latent heat of fusion (ΔH) was calculated using following equation 8:

$$\% \text{ change in latent heat of fusion} = \frac{[\Delta H_{Treated} - \Delta H_{Control}]}{\Delta H_{Control}} \times 100 \quad (8)$$

Where, $\Delta H_{Control}$ and $\Delta H_{Treated}$ are the latent heat of fusion of the control and treated iron sulphate, respectively.

## Results and Discussion

*Powder X-ray Diffraction (PXRD) Analysis*

The PXRD diffractograms of the control and Biofield Energy Treated samples of iron sulphate are given in Figure 1. The diffractograms showed very sharp peaks, which represents the crystalline nature of both the samples. Also, the PXRD data is presented in Table 1, which involves the analysis of Bragg angle (2θ), relative peak intensity (%), and crystallite size (G) for the control and Biofield Energy Treated iron sulphate from the diffractograms. The crystallite size was calculated using Scherer equation [43].

The highest intense peak (100% relative intensity) in the control sample was observed at Bragg's angle (2θ) equal to 18.3° (Table 1, entry 4), while it was observed in the Biofield Energy Treated sample at 2θ equal to 18.1° (Table 1, entry 4). The Bragg's angle (2θ) of the remaining diffraction peaks in both the samples remained almost same, but the relative intensities of the peaks of the Biofield Energy Treated sample were found to be altered compared to the control sample. The relative intensities of the PXRD peaks at 2q equal to 11.1°, 13.1°, 16.2°, 22.1°, 27.4°, 32.8°, 34.2°, 36.9°, and 54.2° (Table 1, entry 1-3, 5, 7-10, and 12) in the Biofield Energy Treated sample were significantly increased in the range from 24.63% to 301.40%, compared to the control sample. Subsequently, the relative intensities of the PXRD peaks at 2q equal to 23.6° and 47.1° (Table 1, entry 6 and 11) in the Biofield Energy Treated sample were significantly decreased by 39.49% and 35.12%, respectively, as compared to the control sample. On the other hand, the crystallite size values of the Biofield Energy Treated sample at 2q equal to 11.1° and 22.1° (Table 1, entry 1 and 5) was significantly reduced by 15.40% and 8.34%, respectively with respect to the control sample. Subsequently, the crystallite size values of the Biofield Energy Treated samples at 2q equal to 13.1°, 18.3/18.1°, 23.6°, 27.4°, 32.8°, 34.2°, 36.9°, and 47.1° (Table 1, entry 2, 4, and 6-11) were significantly increased from 7.71% to 33.36% in the Biofield Energy Treated sample in comparison to the control sample. However, the crystallite size values of the control and Biofield Energy Treated iron sulphate at position 2q equal to 16.2° and 54.2° (Table 1, entry 3 and 12) remained unchanged. Also, the average crystallite size of the Biofield Energy Treated iron sulphate was significantly increased by 4.98%, compared with the control sample.

The significant variations in the crystallite size and relative intensities of the Biofield Energy Treated iron sulphate indicated the modification of the crystal morphology of the sample compared with the control sample. Several studies reported the impact of Biofield Energy Treatment in producing a new crystalline polymorph of the compound by altering the crystal morphology through the changes in the relative intensities and crystallite size of the characteristic diffraction peaks [35-37, 44]. Thus, the Trivedi Effect® - Energy of Consciousness Healing Treatment probably led to produce a new polymorphic form by transferring the energy into iron sulphate sample. The polymorphism plays significant role in the performance of drug, such as its bioavailability, efficacy, and toxicity, due to the alterations in their physicochemical and thermodynamic properties from the original form [45, 46]. Thus, the Biofield Energy Treatment could be considered as a useful method for the production of new polymorph of iron sulphate with improved drug performance.

*Particle Size Analysis (PSA)*

The PSA data revealed the particle sizes (*i.e.,* $d_{10}$, $d_{50}$, $d_{90}$, and D(4,3) ) of the control and Biofield Energy Treated iron sulphate, and the results are

Table 1. PXRD data for the control and Biofield Energy Treated iron sulphate.

| Entry No. | Bragg angle (°2q) | Relative Peak Intensity (%) | | | Crystallite size (G, nm) | | |
|---|---|---|---|---|---|---|---|
| | | Control | Treated | % change [a] | Control | Treated | % change [b] |
| 1 | 11.1 | 2.72 | 3.39 | 24.63 | 31.43 | 26.59 | -15.40 |
| 2 | 13.1 | 2.00 | 5.74 | 187.00 | 28.86 | 34.64 | 20.03 |
| 3 | 16.2 | 7.92 | 21.99 | 177.65 | 34.76 | 34.76 | 0.00 |
| 4 | 18.3/18.1 | 100.0 | 100.0 | 0.00 | 38.73 | 43.57 | 12.50 |
| 5 | 22.1 | 4.66 | 12.29 | 163.73 | 31.88 | 29.22 | -8.34 |
| 6 | 23.60 | 26.06 | 15.77 | -39.49 | 29.30 | 31.96 | 9.08 |
| 7 | 27.40 | 13.22 | 28.34 | 114.37 | 25.30 | 27.25 | 7.71 |
| 8 | 32.80 | 3.98 | 9.85 | 147.49 | 22.42 | 29.90 | 33.36 |
| 9 | 34.20 | 2.15 | 8.63 | 301.40 | 25.72 | 32.74 | 27.29 |
| 10 | 36.90 | 5.02 | 9.98 | 98.80 | 27.91 | 30.24 | 8.35 |
| 11 | 47.10 | 14.38 | 9.33 | -35.12 | 34.21 | 38.49 | 12.51 |
| 12 | 54.20 | 5.23 | 9.64 | 84.32 | 39.64 | 39.64 | 0.00 |

[a]denotes the percentage change in the relative intensity of Biofield Energy Treated sample with respect to the control sample; [b]denotes the percentage change in the crystallite size of Biofield Energy Treated sample with respect to the control sample.

Table 2. Particle size distribution of the control and Biofield Energy Treated iron sulphate

| Test Item | $d_{10}$ (µm) | $d_{50}$ (µm) | $d_{90}$ (µm) | D(4,3) (µm) | SSA($m^2$/Kg) |
|---|---|---|---|---|---|
| Control sample | 146 | 396 | 856 | 457 | 21.75 |
| Biofield Energy Treated sample | 244 | 585 | 1140 | 649 | 13.40 |
| Percent change* (%) | 67.12 | 47.72 | 33.18 | 42.01 | -38.39 |

$d_{10}$, $d_{50}$, and $d_{90}$: particle diameter corresponding to 10%, 50%, and 90% of the cumulative distribution, D (4,3) : the average mass-volume diameter, SSA : the specific surface area; *denotes the percentage change in the particle size distribution of the Biofield Energy Treated sample with respect to the control sample.

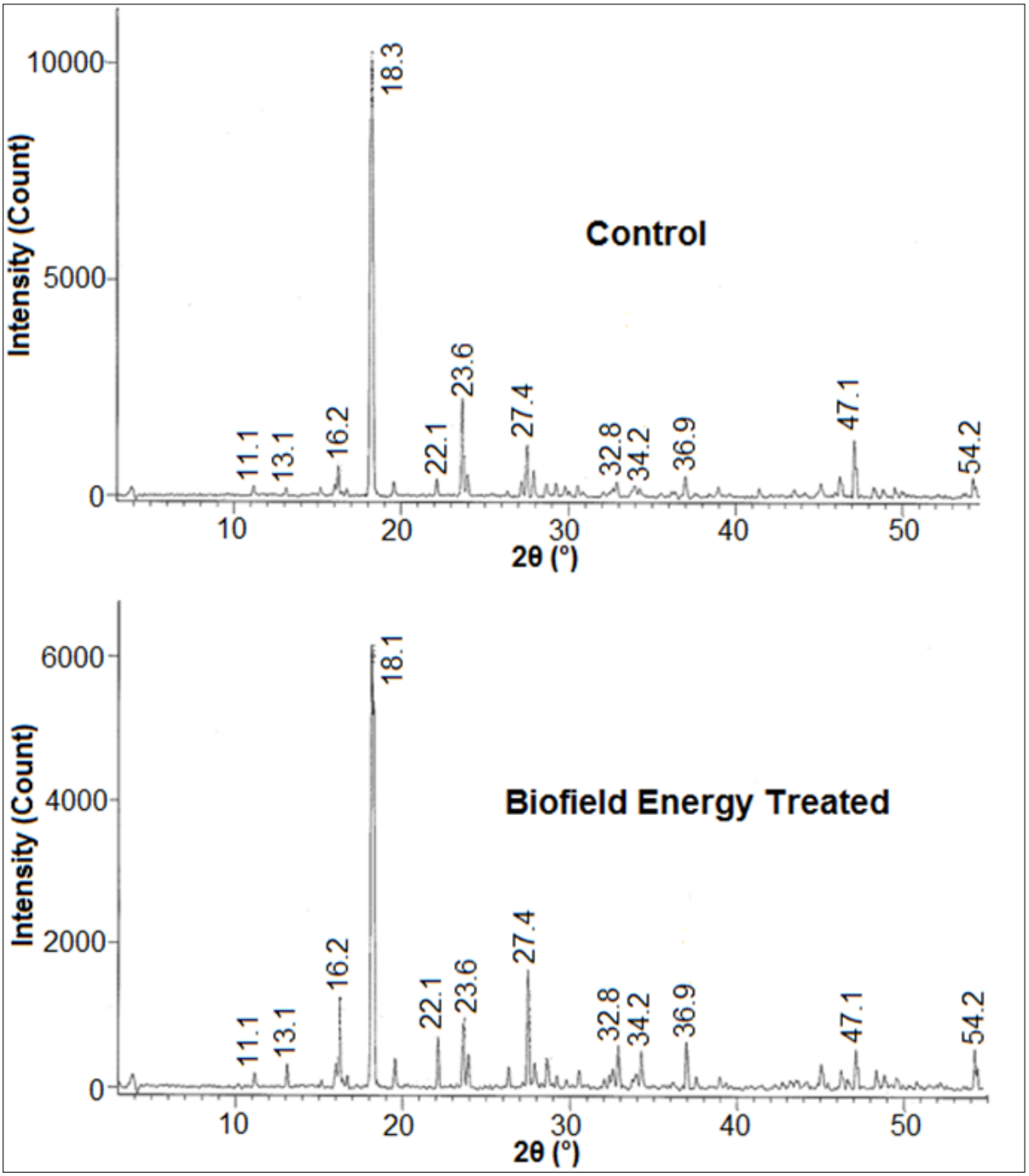


Figure 1. XRD diffractograms of the control and Biofield Energy Treated iron sulphate.

presented in Table 2. From the data, it was observed that the particle sizes at $d_{10}$, $d_{50}$, $d_{90}$, and D(4,3) value of Biofield Energy Treated sample showed a significant increase by 67.12%, 47.72%, 33.18% and 42.01%, respectively, as compared to the control sample. Some studies reported the impact of thermal energy elevation on the particle size. Hence, it might be assumed that the Biofield Energy Treatment may reduce the thermodynamically driving force, which decreases the nucleus densities and ultimately enhances the particle size [47, 48]. The study also analysed the surface area of both samples and the results are presented in the Table 2. It shows that the surface area of Biofield Energy Treated sample (13.40 $m^2$/kg) was significantly reduced by 38.39% compared to the surface area of the control sample (21.75 $m^2$/kg). The reduced surface area of the Biofield Energy Treated sample might be due to the increase in particle size of the treated sample after the Biofield Energy Treatment. The increased particle size of the compound may be useful in improving its appearance, shape and flowability [49, 50]. Thus, the Biofield Energy Treatment may be used to improve the powder flowability of iron sulphate .

*Ultraviolet-Visible Spectroscopy (UV-Vis) Analysis*

The UV-visible spectra of the control and treated iron sulphate samples are shown in the Figure 2. The UV spectrum of the control and biofield energy treated samples showed the maximum absorbances at 190 nm ($\lambda_{max}$). The peak at 190 nm was showed a minor shift of absorbance maxima from 0.6367 in the control sample to 0.6129 in the Biofield Energy Treated sample. The analysis represents that there might not be any significant change in the electronic transitions between highest occupied molecular orbital and lowest unoccupied molecular orbital, induced by the Biofield Energy Treatment.

*Fourier Transform Infrared (FT-IR) Spectroscopy*

The FT-IR spectra of the control and treated samples of iron sulphate are shown in Figure 3. The FT-IR spectra of both control and Biofield Energy Treated sample showed the clear stretching and bending peak that are matched well with the available literature [51, 52]. The transitions include the stretching and bending modes of O—H and H—O—H bonds, and stretching vibrations of the $SO_4$ group. According to the literature, the stretching O—H vibrations (vOH) takes place at 2900-3660 $cm^{-1}$ and M—O—H bending vibrations (δOH) at 900-1170 $cm^{-1}$ [53]. In these spectra, the broad peaks were observed near 3342 and 3378 $cm^{-1}$ in the functional group area of the control and Biofield Energy Treated samples, respectively, due to the presence of O—H vibrations of water molecules. The spectra showed S=O stretching at 1094 and 1095 $cm^{-1}$ for the control and Biofield Energy Treated samples, respectively. The FT-IR spectra of both samples did not display any alteration in the vibrational frequencies, which represents that there was no alteration in the structural properties associated with a change in dipole moment in the molecule in the Biofield Energy Treated sample as compared to the control sample [54].

*Thermal Gravimetric Analysis (TGA) / Differential Thermogravimetric Analysis (DTG)*

The TGA/DTG thermograms represent the thermal stability of the control and treated samples of iron sulphate (Figures 4 and 5). The TGA thermograms of the control and treated samples exhibited three steps thermal degradation (Figure 4 and Table 3). The thermogram pattern was matched with the literature, according to which, the first and second steps of weight loss might occur due to the loss of water molecules from iron sulphate heptahydrate ($FeSO_4 \bullet 7H_2O$). Consequently, the final major weight loss takes place due to the oxidation as well as dehydration of the other part of monohydrate, sulphate decomposition [55, 56]. The data represents that the control sample lost weight by 42.8, 6.96, and 23.46% in 1st, 2nd and 3rd steps of degradation, respectively (Table 3). However, the Biofield Energy Treated sample lost weight by 40.31, 5.84, and 25.05% in 1st, 2nd and 3rd steps of degradation, respectively (Table 3). Thus, it revealed that the weight loss of Biofield Energy Treated sample in the first and second step was reduced by 5.82% and 16.09%, respectively, whereas, in third step, it was increased by 6.78%, compared to the control sample. Also, the overall weight loss of the Biofield Treated sample was reduced by 2.76% as compared to the control sample during this process. It represents that the thermal stability of the Biofield Energy Treated sample was increased as compared to the control iron

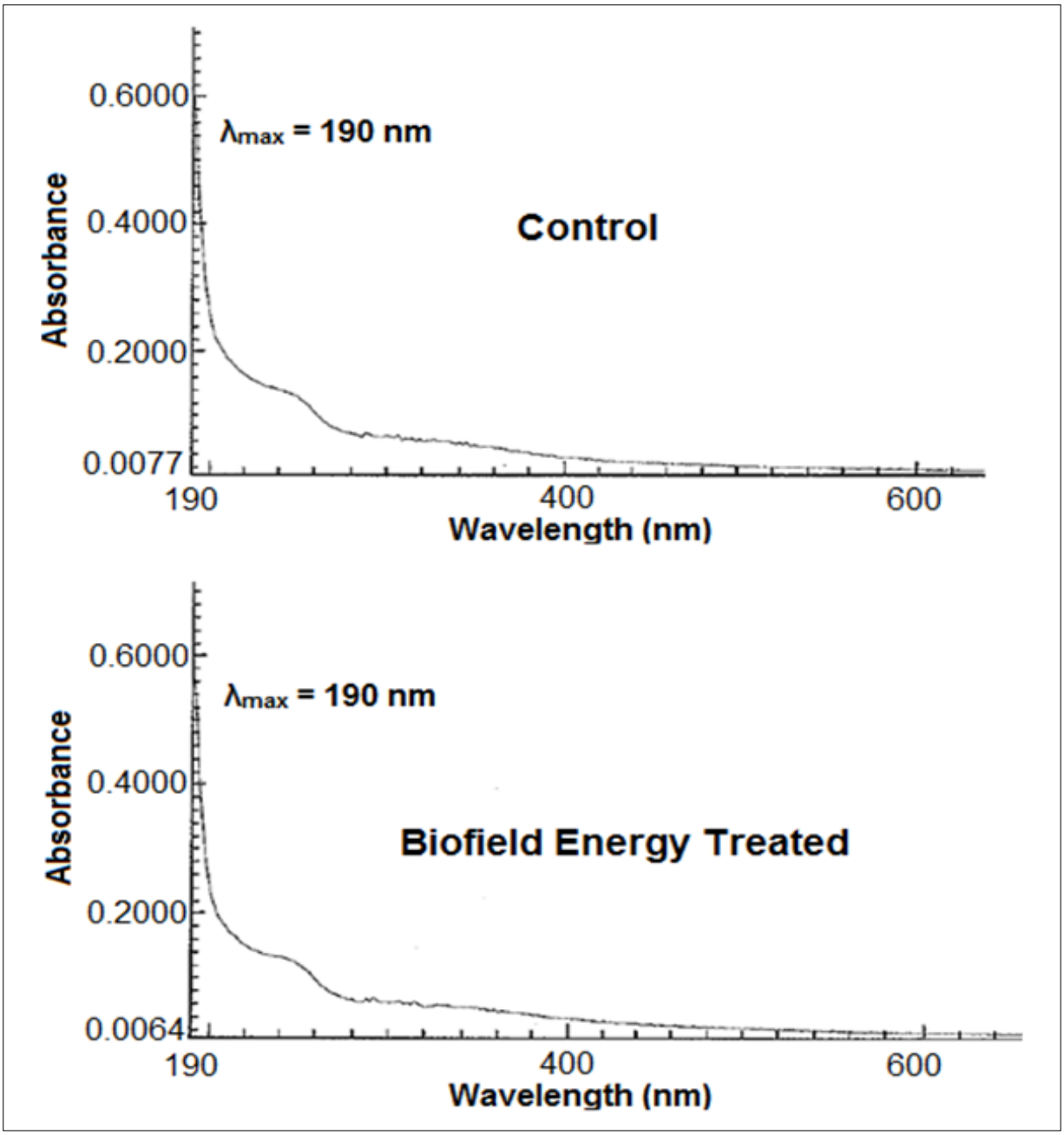


Figure 2. UV-vis spectra of the control and Biofield Energy Treated iron sulphate.

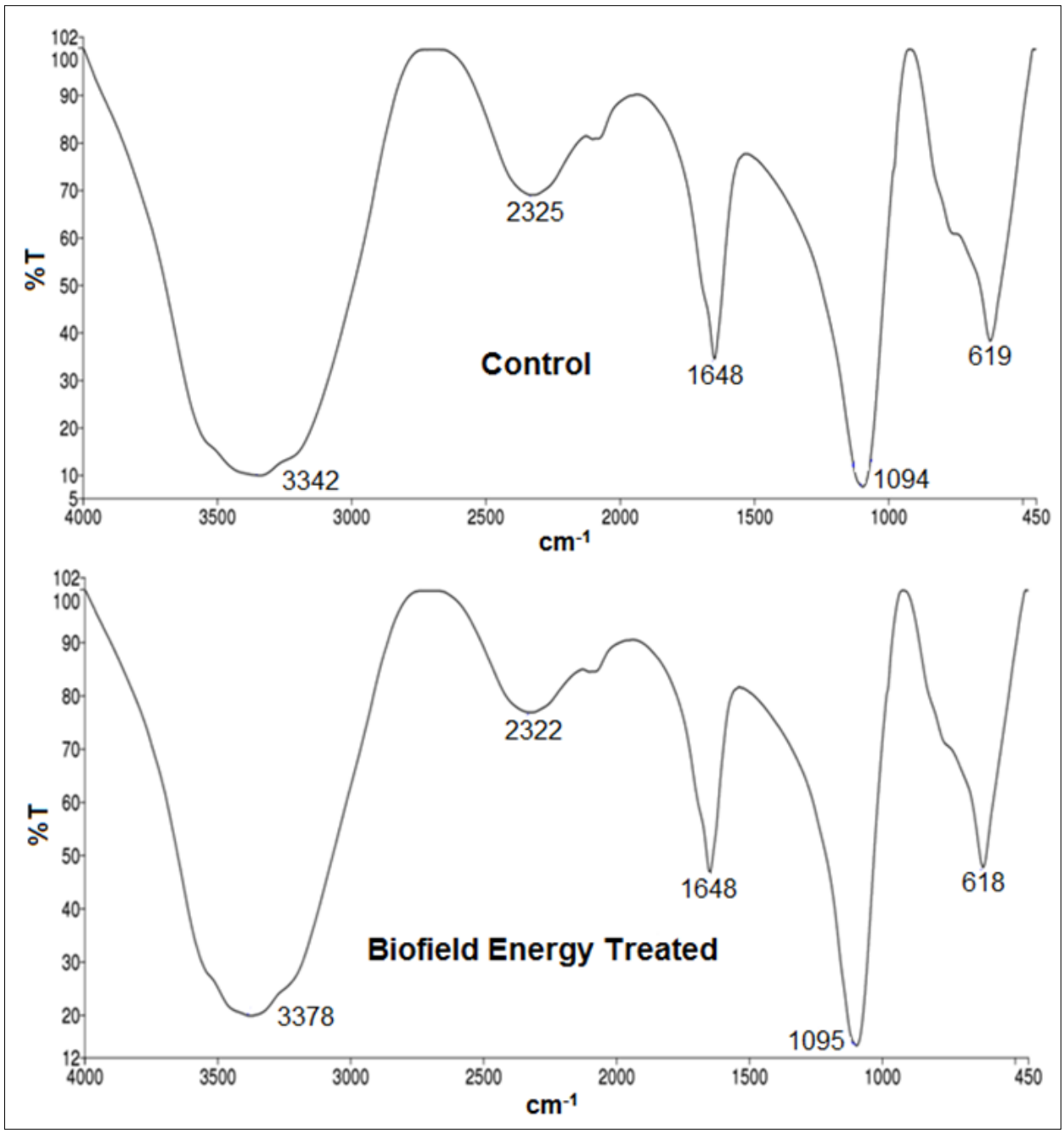


Figure 3. FT-IR spectra of the control and Biofield Energy Treated iron sulphate.

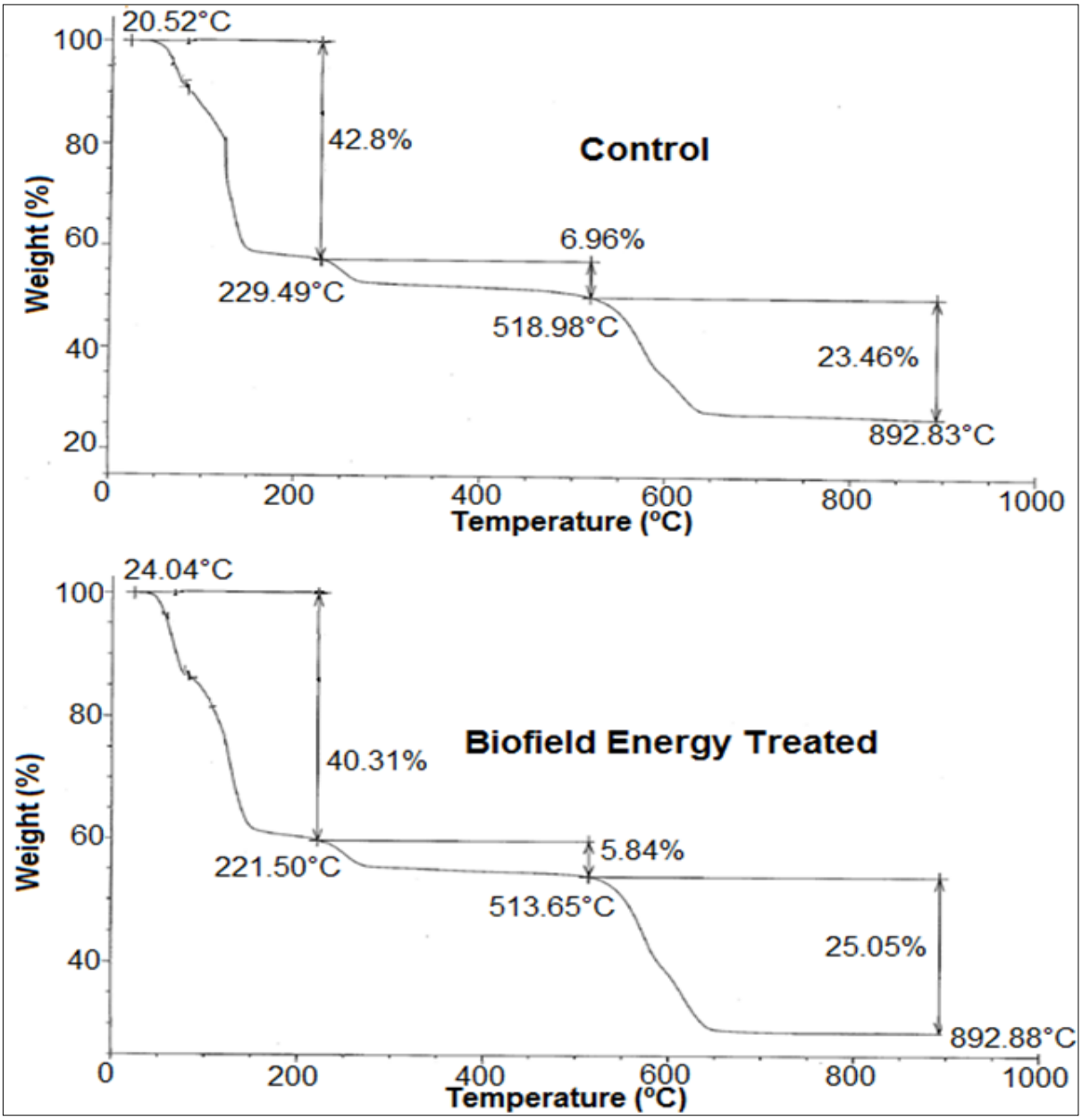


Figure 4. TGA thermograms of the control and Biofield Energy Treated iron sulphate

Table 3. Thermal degradation steps of the control and Biofield Energy Treated iron sulphate.

| Step | Temperature (°C) | | | Weight loss % | | % Change * |
|---|---|---|---|---|---|---|
| | Control | Treated | | Control | Treated | |
| 1st step of degradation | 229.49 | 221.5 | | 42.8 | 40.31 | -5.82 |
| 2nd step of degradation | 518.98 | 513.65 | | 6.96 | 5.84 | -16.09 |
| 3rd step of degradation | 892.83 | 892.88 | | 23.46 | 25.05 | 6.78 |

*denotes the percentage change in the weight loss of Biofield Energy Treated sample with respect to the control sample.

sulphate sample, which might be due to the increase in particle size of the treated sample [57].

The DTG thermograms of both the control and Biofield Energy Treated samples (Figure 5) exhibited three peaks. The analysis revealed that the maximum thermal degradation temperature ($T_{max}$) of 1st and 4th peaks of the Biofield Energy Treated sample were reduced by 2.57% and 0.41%, respectively, as compared to the control sample (Table 4). Besides, the $T_{max}$ of 2nd and 3rd peaks of the Biofield Energy Treated sample were slightly increased by 0.29% and 0.35%, compare to the control sample (Table 4). Overall, the TGA/DTG analysis revealed that the thermal stability of the Biofield Energy Treated iron sulpahte was altered as compared to the control sample, which might be due to the alteration in particle size of the treated sample after the Biofield Energy Treatment.

*Differential Scanning Calorimetry (DSC) Analysis*

The DSC thermograms of the control and Biofield Energy Treated samples of iron sulphate are presented in Figure 6. Some studies reported the dehydration behavior of a hydrated iron salt by using DSC and TGA techniques [55, 56]. According to this, the DSC thermogram of iron sulphate heptahydrate shows three peaks, when heated at the rate of 10 °C under nitrogen atmosphere. Among these peaks, first peak was observed at temperature <100 °C ($FeSO_4 \bullet 7H_2O \rightarrow FeSO_4 \bullet 4H_2O$), second peak at 85 to 149 °C ($FeSO_4 \bullet 4H_2O \rightarrow FeSO_4 \bullet H_2O$), and third peak at 247 to 342 °C ($FeSO_4 \bullet H_2O \rightarrow FeSO_4$) due to the dehydration of water molecules. They also concluded that accurate thermal data from the TGA/DSC dehydration experiments depends on various factors like proper selection of the heating rate, particle size, open or closed pan, etc. [55]. Table 5

In this study, the DSC thermogram of the control iron sulphate heptahydrate (Figure 6) showed the presence of the four endothermic peaks. The 1st sharp endothermic peak was observed at 75.83 °C, which was may be due to the melting point of iron sulphate heptahydrate. However, the temperature of this peak (69.58 °C ) was significantly decreased in Biofield Energy Treated sample by 8.24% with a significant reduction in the latent heat of fusion (ΔH) by 92.29% (Table 3), compared with the control sample. The 2nd broad endothermic peak at 95.06 °C in control sample was might be due to the dehydration of two molecules of water from $FeSO_4 \bullet 6H_2O$. Further, the temperature of this peak was also significantly reduced

Table 4. Derivative thermal degradation steps of the control and Biofield Energy Treated samples of iron sulphate.

| Description | $T_{max}$(°C) | | | |
|---|---|---|---|---|
| | $P_1$ (°C) | $P_2$ (°C) | $P_3$ (°C) | $P_4$ (°C) |
| Control Sample | 66.54 | 125.45 | 250.81 | 576.06 |
| Biofield Energy Treated | 64.83 | 125.82 | 251.68 | 573.68 |
| %Change* | -2.57 | 0.29 | 0.35 | -0.41 |

$P_1$, $P_2$, $P_3$, and $P_4$: peak 1, 2, 3, and 4. *denotes the percentage change of the Biofield Energy Treated sample with respect to the control sample, $T_{max}$ = the temperature at which maximum weight loss takes place in TG or peak temperature in DTA.

Table 5. Comparison of DSC data between the control and Biofield Energy Treated iron sulphate.

| Sample | Melting Temperature (°C) | | | | ΔH(J/g) | | | |
|---|---|---|---|---|---|---|---|---|
| | 1st Peak | 2nd Peak | 3rd Peak | 4th Peak | 1st Peak | 2nd Peak | 3rd Peak | 4th Peak |
| Control | 75.83 | 95.06 | 115.81 | 273.13 | 116.9 | 76.79 | 500.5 | 254.2 |
| Biofield Energy Treated | 69.58 | 76.72 | 121.10 | 271.48 | 9.01 | 10.53 | 805.4 | 270.4 |
| % Change* | -8.24 | -19.29 | 4.57 | -0.61 | -92.29 | -86.29 | 60.92 | 6.37 |

ΔH: Latent heat of fusion, *denotes the percentage change of the Biofield Energy Treated sample with respect to the control sample.

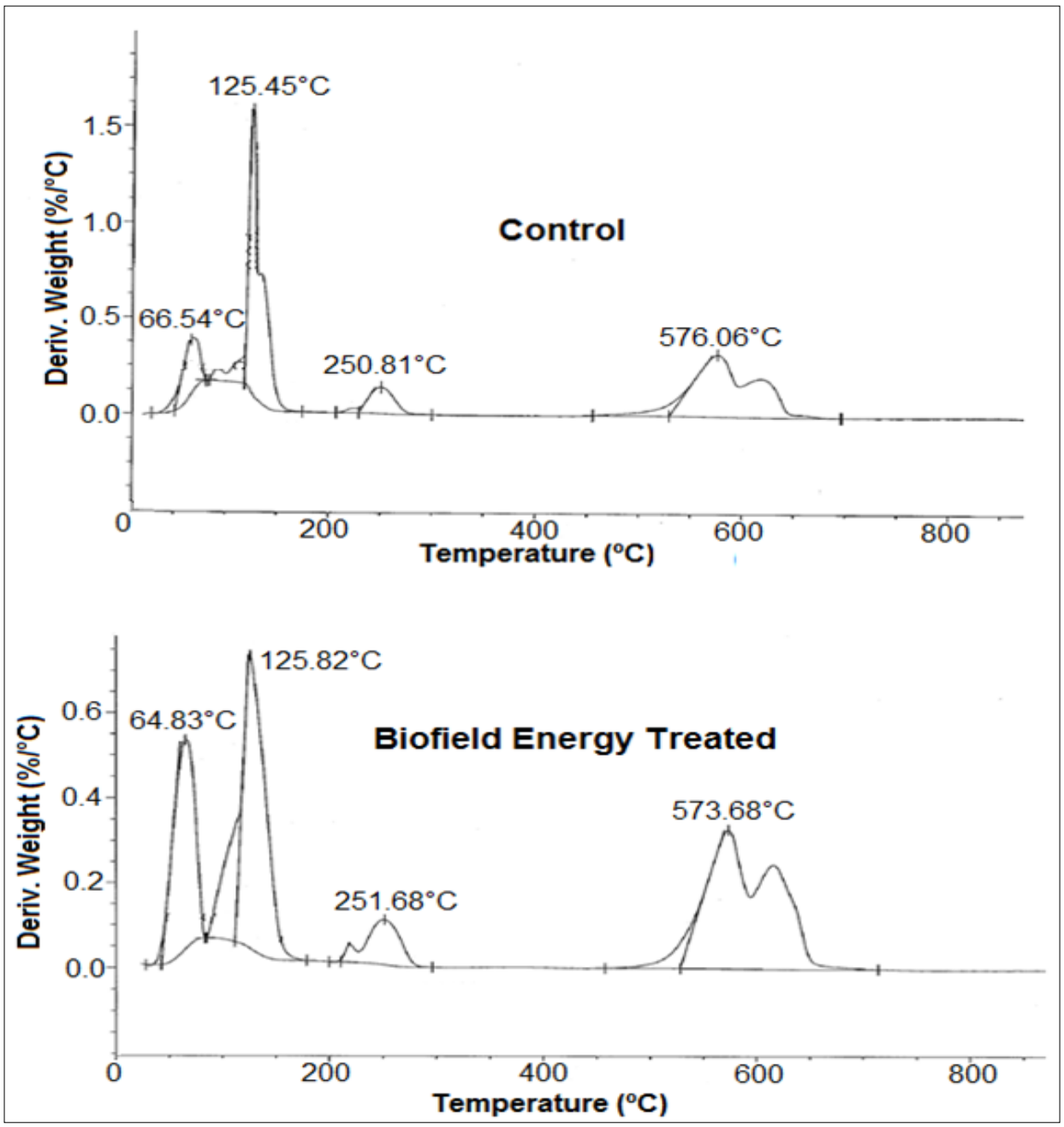


Figure 5. DTG thermograms of the control and Biofield Energy Treated iron sulphate.

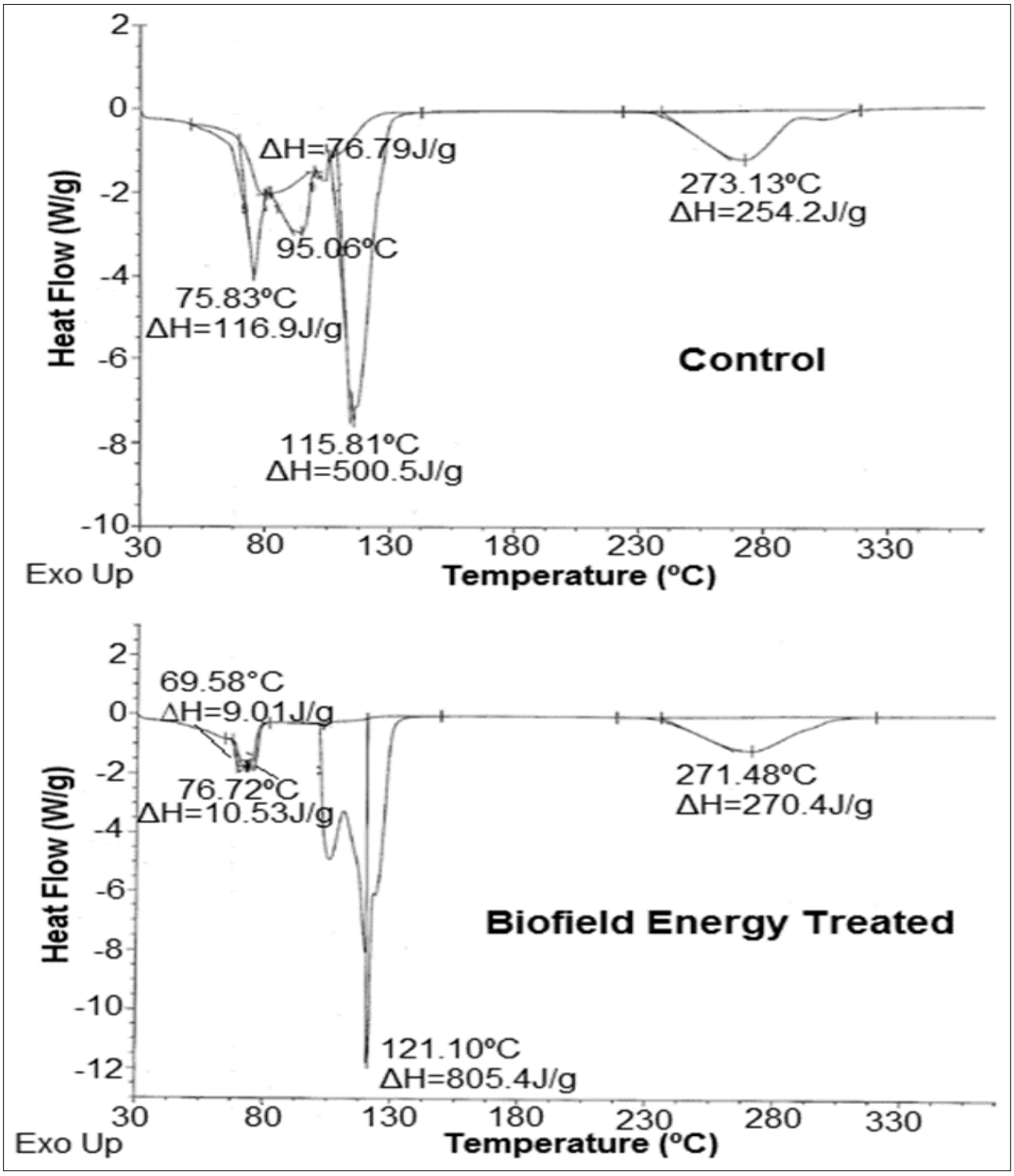


Figure 6. DSC thermograms of the control and Biofield Energy Treated iron sulphate.

by 19.29% in the Biofield energy Treated sample (76.72°C) along with reduction in ΔH by 86.29%, compared with the control sample. Later on, the melting temperature of the 3rd sharp endothermic peak (due to removal of three water molecules) was increased in the Biofield Energy Treated sample (121.10°C) by 4.57% with a significant 60.92% increase in ΔH, compared with the control sample (115.81 °C). Finally, a broad endothermic peak was observed at 273.13°C in the control sample (due to dehydration of iron sulphate in anhydrous form), which was slightly reduced by 0.61% in the Biofield Energy Treated sample (271.48°C) along with 6.37% enhancement in ΔH as compared with the control sample (Table 3). The overall latent heat of fusion on the Biofield Energy Treated sample (1095.34 J/g) was significantly increased by 15.49% compared with the control sample (948.39 J/g). The alteration in the latent heat of fusion may be due to the changes in the molecular chains and crystal structures [55, 57]. Thus, it is assumed that the Biofield Energy Treatment may alter the thermal stability of iron sulphate by impacting the crystal morphology, molecular chain structures and particle sizes.

## Conclusions

The overall study concluded that the Trivedi Effect® - Energy of Consciousness Healing Treatment has the striking ability to modify the physicochemical and thermal properties of iron sulphate. The PXRD analysis revealed that the relative intensities of the characteristic peaks were significantly changed from -39.49 to 301.40% in the Biofield Energy Treated sample, compared to the control sample. Also, the crystallite sizes corresponding to these peaks in the Biofield Energy Treated sample also showed alteration in the range from -15.40 to 33.36% along with 4.98% increase in the average crystallite size, compared with the control sample. This analysis might indicate the presence of a different polymorphic form of iron sulphate after the Biofield Energy Treatment. Moreover, the particle sizes at $d_{10}$, $d_{50}$, $d_{90}$ and D(4,3) in the Biofield Energy Treated sample were significantly increased by 67.12%, 47.72%, 33.18% and 42.01%, respectively, along with 38.39% reduction in the specific surface area compared with the control sample. Although, the spectral analysis of the Biofield energy Treated sample did not revealed any change; but the thermodynamic profile showed significant alterations as compared to the control sample. The TGA thermograms of both the samples presented three steps of thermal degradation. Among these steps, the weight loss of Biofield Energy Treated sample in the first and second step was reduced by 5.82% and 16.09%, respectively, compared with the control sample. However, in the third step, it was increased by 6.78%; but the total weight loss of the treated sample was reduced by 2.76%, compared to the control sample. The melting temperature of the Biofield Energy Treated iron sulphate sample was decreased by 8.24, 19.29, and 0.61%, in the 1st, 2nd and 4th peaks respectively, while increased by 4.57% in the 3rd peak, compared with the control sample. The latent heat of fusion (ΔH) in 1st, 2nd, 3rd and 4th peaks corresponding to the transitions from $FeSO_4 \bullet 7H_2O$ to $FeSO_4$ of the Biofield Energy Treated sample also showed alterations by -92.29, -86.29, 60.92, and 6.37%, respectively, compared with the control sample. Overall, the thermal analysis revealed that the thermal stability of the Biofield Energy Treated iron sulphate was increased compared to the control sample. Thus, the Trivedi Effect®-Consciousness Energy Healing Treatment might yield a polymorphic form of iron sulphate having increased crystallite size, particle size and thermodynamic stability, which may help in improving the appearance, safety, efficacy and stability of the iron sulphate formulation compared with the control sample. The Biofield Energy Treated iron sulphate might be helpful in designing the better nutraceutical/pharmaceutical formulations, with improved therapeutic response against the problems associated with iron deficiency.

## Acknowledgements

The authors are grateful to GVK Biosciences Pvt. Ltd., Trivedi Science, Trivedi Global, Inc., Trivedi Testimonials, and Trivedi Master Wellness for their assistance and support during this work.

## References

1. Geisser P, Burckhardt S (2011). The pharmacokinetics and pharmacodynamics of iron preparations. Pharmaceutics 3: 12-33.
2. Zimmermann MB, Hurrell RF (2007) Nutritional iron deficiency. Lancet 370: 511-520.

3. Usha R, (2000) Functional consequences of nutritional anemia during pregnancy and early childhood In: Nutritional Anemias. CRC Press, Taylor & Francis Group.

4. Goddard AF, James MW, McIntyre AS, Scott BB (2011) Guidelines for the management of iron deficiency anaemia. Gut 60: 1309-1316.

5. Gotloib L, Silverberg D, Fudin R, Shostak A (2006) Iron deficiency is a common cause of anemia in chronic kidney disease and can often be corrected with intravenous iron. J Nephrol 19: 161-167.

6. Nanas PN, Matsouka C, Karageorgopoulos D, Leonti A, Tsolakis E, Drakos SG, Tsagalou EP, Maroulidis GD, Alexopoulos GP, Kanakakis JE, Anastasiou-Nana MI (2006) Etiology of anemia in patients with advanced heart failure. J Amer Coll Cardiol 48: 2485-2489.

7. Gasche C, Lomer MCE, Cavill I, Weiss G (2004) Iron, anaemia, and inflammatory bowel diseases. Gut 53: 1190-1197.

8. Dawson PA (2013) Role of sulphate in development. Reproduction 146: R81-R89.

9. Lay KM, Oshiro R, Arasaki C, Ashizawa K, Tatemoto H (2011) Role of acidification elicited by sialylation and sulfation of zona glycoproteins during oocyte maturation in porcine sperm–zona pellucida interactions. J Reprod Develop 57: 744-751.

10. Appel LJ, Baker DH, Bar-Or O, Minaker KL, Morris RC, Resnick LM, Sawka MN, Volpe SI, Weinberger MH, Whelton PK (2004) Sulfate. In: Dietary Reference Intakes for Water Potassium, Sodium, Chloride and Sulfate. The National Academies Press: Washington DC, USA.

11. Allen HE, Halley-Henderson MA, Hass CN (1989) Chemical composition of bottled mineral water. Arch Environ Health 44: 102-116.

12. Florin THJ, Neale G, Goretski S, Cummings JH (1993) The sulfate content of foods and beverages. J Food Comp Anal 6: 140-151.

13. Bannerman J, Campbell NRC, Hasinoff BB, Venkataram S (1996) The dissolution of iron from various commercial preparations. Pharm Acta Helv 71: 129-133.

14. Walker SE, Paton TW, Cowan DH, Manuel MA, Dranitsaris G (1989) Bioavailability of iron in oral ferrous sulfate preparations in healthy volunteers. CMAJ 141: 543-547.

15. Zariwala MG, Somavarapu S, Farnaud S, Renshaw D (2013) Comparison study of oral iron preparations using a human intestinal model. Sci Pharm 81: 1123-1139.

16. Stenger VJ (1999) Bioenergetic Fields. The Scientific Review of Alternative Medicine 3.

17. Rogers M (1989) Nursing: A Science of Unitary Human Beings. In: Riehl-Sisca JP (ed) Conceptual Models for Nursing Practice. 3rd edn. Norwark: Appleton & Lange.

18. Warber SL, Cornelio D, Straughn, J, Kile G (2004) Biofield energy healing from the inside. J Altern Complement Med 10: 1107-1113.

19. Sances F, Flora E, Patil S, Spence A, Shinde V (2013) Impact of biofield treatment on ginseng and organic blueberry yield. Agrivita 35: 22-29.

20. Jain S, Hammerschlag R, Mills P, Cohen L, Krieger R, Vieten C, Lutgendorf S (2015) Clinical studies of biofield therapies: Summary, methodological challenges, and recommendations. Glob Adv Health Med 4: 58-66.

21. Koithan M (2009) Introducing complementary and alternative therapies. J Nurse Pract 5: 18-20.

22. Trivedi MK, Patil S, Shettigar H, Mondal SC, Jana S (2015) *In vitro* evaluation of biofield treatment on *Enterobacter cloacae*: Impact on antimicrobial susceptibility and biotype. J Bacteriol Parasitol 6: 241.

23. Trivedi MK, Branton A, Trivedi D, Nayak G, Mondal SC, Jana S (2015) Evaluation of antibiogram, genotype and phylogenetic analysis of biofield treated *Nocardiaotitidis*. BiolSyst Open Access 4: 143.

24. Trivedi MK, Branton A, Trivedi D, Nayak G, Gangwar M, Jana S (2015) Antibiogram, biochemical reactions, and genotypic pattern of biofield treated *Pseudomonas aeruginosa*. J Trop Dis 4: 181.

25. Trivedi MK, Patil S, Shettigar H, Mondal SC, Jana S (2015) The potential impact of biofield treatment on

human brain tumor cells: A time-lapse video microscopy. J Integr Oncol 4: 141.

26. Trivedi MK, Branton A, Trivedi D, Nayak G, Mondal SC, Jana S (2015) Evaluation of biochemical marker - glutathione and DNA fingerprinting of biofield energy treated *Oryza sativa*. American Journal of BioScience 3: 243-248.
27. Trivedi MK, Branton A, Trivedi D, Nayak G, Gangwar M, Jana S (2016) Molecular analysis of biofield treated eggplant and watermelon crops. Adv Crop Sci Tech 4: 208.
28. Trivedi MK, Branton A, Trivedi D, Nayak G, Mondal SC, Jana S (2015) Morphological characterization, quality, yield and DNA fingerprinting of biofield energy treated alphonso mango (*Mangifera indica L.*). Journal of Food and Nutrition Sciences 3: 245-250.
29. Trivedi MK, Branton A, Trivedi D, Nayak G, Mishra RK, Jana S (2015) Physicochemical evaluation of biofield treated peptone and malmgren modified terrestrial orchid medium. American Journal of Bioscience and Bioengineering 3: 169-177.
30. Trivedi MK, Branton A, Trivedi D, Nayak G, Singh R, Jana S (2015) Physicochemical characterization of biofield treated orchid maintenance/replate medium. Journal of Plant Sciences. 3: 285-293.
31. Trivedi MK, Patil S, Tallapragada RM (2013) Effect of biofield treatment on the physical and thermal characteristics of silicon, tin and lead powders. J Material SciEng 2: 1-7.
32. Trivedi MK, Nayak G, Patil S, Tallapragada RM, Latiyal O, Jana S (2015) Evaluation of biofield treatment on physical and structural properties of bronze powder. AdvAutomobEng 4: 119.
33. Trivedi MK, Branton A, Trivedi D, Nayak G, Bairwa K, Jana S (2015) Spectroscopic characterization of disulfiram and nicotinic acid after biofield treatment. J Anal Bioanal Tech 6: 265.
34. Trivedi MK, Patil S, Shettigar H, Singh R, Jana S (2015) An impact of biofield treatment on spectroscopic characterization of pharmaceutical compounds. Mod ChemAppl 3: 159.
35. Trivedi MK, Branton A, Trivedi D, Nayak G, Balmer AJ, Anagnos D, Kinney JP, Holling JM, Balmer JA, Duprey-Reed LA, Parulkar VR, Panda P, Sethi KK, Jana S (2017) Evaluation of physicochemical, thermal, structural, and behavioral properties of magnesium gluconate treated with energy of consciousness (The Trivedi Effect®). Journal of Drug Design and Medicinal Chemistry3: 5-17.
36. Trivedi MK, Branton A, Trivedi D, Nayak G, Balmer AJ, Anagnos D, Kinney JP, Holling JM, Balmer JA, Duprey-Reed LA, Parulkar VR, Panda P, Sethi KK, Jana S (2017) Study of the energy of consciousness healing treatment on physical, structural, thermal, and behavioral properties of zinc chloride. Modern Chemistry 5: 19-28.
37. Trivedi MK, Branton A, Trivedi D, Nayak G, Balmer AJ, Anagnos D, Kinney JP, Holling JM, Balmer JA, Duprey-Reed LA, Parulkar VR, Panda P, Sethi KK, Jana S (2017) Evaluation of physicochemical, spectral, thermal and behavioral properties of the biofield energy healing treated sodium selenate. Science Journal of Chemistry5: 12-22.
38. Trivedi MK, Branton A, Trivedi D, Nayak G, Saikia G, Jana S (2015) Thermal, spectroscopic and chromatographic characterization of biofield energy treated benzophenone. Science Journal of Analytical Chemistry 3: 109-114.
39. Trivedi MK, Patil S, Mishra RK, Jana S (2015) Structural and physical properties of biofield treated thymol and menthol. J Mol Pharm Org Process Res 3: 127.
40. Trivedi MK, Tallapragada RM, Branton A, Trivedi D, Nayak G, Mishra RK, Jana S (2015) Characterization of Physical, Spectroscopic and Thermal Properties of Biofield Treated Biphenyl. American Journal of Chemical Engineering. 3: 58-65.
41. Trivedi MK, Branton A, Trivedi D, Nayak G, Lee AC, Hancharuk A, Sand CM, Schnitzer DJ, Thanasi R, Meagher EM, Pyka FA, Gerber GR, Stromsnas JC, Shapiro JM, Streicher LN, Hachfeld LM, Hornung MC, Rowe PM, Henderson SJ, Benson SM, Holmlund ST, Salters SP, Panda P, Jana S (2017) A comprehensive analytical evaluation of the Trivedi Effect® - Energy of Consciousness Healing Treatment on the physical, structural, and thermal properties of zinc chloride. American Journal of Applied Chemistry 5: 7-18.

42. Trivedi MK, Branton A, Trivedi D, Nayak G, Plikerd WD, Surguy PL, Kock RJ, Piedad RB, Callas RP, Ansari SA, Barrett SL, Friedman S, Christie SL, Chen Liu S-M, Starling SE, Jones S, Allen SM, Wasmus SK, Benczik TA, Slade TC, Orban T, Vannes VL, Schlosser VM, Albino YSY, Panda P, Sethi KK, Jana S (2017) A systematic study of the biofield energy healing treatment on physicochemical, thermal, structural, and behavioral properties of iron sulphate. International Journal of Bioorganic Chemistry. 2: 135-145.

43. Langford JI, Wilson AJC (1978) Scherrer after sixty years: A survey and some new results in the determination of crystallite size. J Appl Cryst 11: 102-113.

44. Brittain HG (2009) Polymorphism in pharmaceutical solids in Drugs and Pharmaceutical Sciences, volume 192, 2nd Edn, Informa Healthcare USA, Inc., New York.

45. Censi R, Martino PD (2015) Polymorph impact on the bioavailability and stability of poorly soluble drugs. Molecules 20: 18759-18776.

46. Zhao Z, Xie M, Li Y, Chen A, Li G, Zhang J, Hu H, Wang X, Li S (2015) Formation of curcumin nanoparticles via solution-enhanced dispersion by supercritical $CO_2$. Int J Nanomedicine 10: 3171-3181.

47. Rashidi AM, Amadeh A (2009) The effect of saccharin addition and bath temperature on the grain size of nanocrystalline nickel coatings. Surf Coat Technol 204: 353-358.

48. Katayama M (1956) The crystal structure of an unstable form of chloroacetamide. Acta Crystallogr 9: 986-991.

49. Mosharrof M, Nystrom C (1995) The effect of particle size and shape on the surface specific dissolution rate of microsized practically insoluble drugs. Int J Pharm 122: 35-47.

50. Buckton G, Beezer AE (1992) The relationship between particle size and solubility. Int J Pharmaceutics 82: R7-R10.

51. Smith AL (1982) The Coblentz Society Desk Book of Infrared Spectra. In: Carver CD (ed) The Coblentz Society Desk Book of Infrared Spectra, (2nd edn) The Coblentz Society: Kirkwood.

52. Majzlan J, Alpers CN, Koch CB, McCleskey RB, Myneni SCB, Neil JM (2011) Vibrational, X-ray absorption, and Mössbauer spectra of sulfate minerals from the weathered massive sulfide deposit at Iron Mountain, California. Chem Geol 284: 296-305.

53. Ryskin YI (1974) The vibrations of protons in minerals: Hydroxyl, water, and ammonium. In: Farmer VC (ed) The Infrared Spectra of Minerals: Mineralogical Society: London.

54. Harris DC, Bertolucci MD (1978) Symmetry and spectroscopy. An introduction to vibrational and electronic spectroscopy. Dover Publications, Inc: New York.

55. Wang T, Debelak KA, Roth JA (2007) Dehydration of iron (II) sulfate heptahydrate. Thermochimica Acta 462: 89-93.

56. Foldvari M (2011) Handbook of thermogravimetric system of minerals and its use in geological practice. Vol. 213, Occasional Papers of the Geological Institute of Hungary, Budapest.

57. Zhang M, Efremov MY, Schiettekatte F, Olson EA, Kwan AT, Lai SL, Wisleder T, Greene JE, Allen LH (2000) Size-dependent melting point depression of nanostructures: Nanocalorimetric measurements. Phys Rev B 62: 10548.